Available online at www.sciencedirect.com
SCIENCE DIRECT®
International Journal of Heat and Mass Transfer 48 (2005) 1145–1154
International Journal of HEAT and MASS TRANSFER
www.elsevier.com/locate/ijhmt

3D modelling of radiative heat transfer in circulating fluidized bed combustors: influence of the particulate composition

Yulong Hua [a,b], Gilles Flamant [a,*], Jidong Lu [b], Daniel Gauthier [a]

[a] Processes, Materials and Solar Energy Laboratory (PROMES-CNRS), BP 5, 66125 Odeillo-Font-Romeu Cédex, France
[b] National Laboratory of Coal Combustion, Huazhong University of Science and Technology, Wuhan, Hubei 430074, China

Received 22 January 2004; received in revised form 30 August 2004
Available online 16 December 2004

Abstract

A three-dimensional model is developed to predict the bed-to-wall radiative heat transfer coefficient in the upper dilute zone of circulating fluidized bed (CFB) combustors. The radiative transfer equation is solved by the discrete ordinates method and Mie scattering theory is applied to calculate the absorption and scattering efficiency factors of particles existing in CFB combustors. Empirical correlations calculate both spacial variation of solid volume fraction and temperature distribution at the wall. The model considers the influences of the particle properties (including particle size distribution, particle optical constants and solid composition) on the radiative heat transfer coefficient. Simulation results show that the particle properties have significant influences on the bed-to-wall radiative heat transfer coefficient in CFB combustors. A very good agreement of predicted results is shown with experimental data.

Keywords: Circulating fluidized bed; Radiative heat transfer; Discrete ordinates method; Particle size; Optical constants

1. Introduction

Radiation is a major component of heat transfer in circulating fluidized beds (CFBs) especially at high temperature (>700 °C) and low bed density (<30 kg/m^3) [1,2]. Hence, the accurate prediction of this heat transfer mechanism is a key issue in the design, operation and optimization of industrial combustors.

Several models had been proposed for estimating the radiation heat transfer component in CFBs. Kudo et al. [3] developed a combined two-dimensional convection–radiation model in which radiation was calculated using the Monte Carlo method. Luan et al. [4] presented the radiative model using the discrete ordinates method. Others [5–10] developed various one-dimensional theoretical models to calculate the radiation in high temperature CFBs. But few works paid attention to the scattering and absorption efficiency factors of the particles existing in industrial CFB combustors, although these factors depend on the particle size and the particle material (i.e., the complex index of refraction, $m = n - ik$) [11].

Because of the on-going combustion, particles in combustors change during the process all the time [12,13]. First, the hydrogen content of coal is converted into water vapor in a relatively short time as the volatile matter burns. Over a longer time span, fixed carbon is oxidized to carbon dioxide during char burnout. Fly

* Corresponding author. Tel.: +33 4 68 30 7758; fax: +33 4 68 30 2940.
E-mail address: flamant@promes.cnrs.fr (G. Flamant).

0017-9310/$ - see front matter © 2004 Elsevier Ltd. All rights reserved.
doi:10.1016/j.ijheatmasstransfer.2004.10.001

Nomenclature

a	particle radius
d_p	particle diameter
$\bar{d}$	particle mean diameter
f_v	solid volume fraction
g	the asymmetry factor
h_r	radiative heat transfer coefficient
h	height variable above air distributor
H	total height of the CFB combustor
i	$\sqrt{-1}$
I	radiation intensity
k	absorption index
m	complex index of refraction ($m = n - ik$)
n	refractive index
N	particle number
Q_{abs}	absorption efficiency factor
Q_{ext}	extinction efficiency factor
Q_{sca}	scattering efficiency factor
Re_p	Reynolds number, defined as $u_g\rho_g d_p/\mu_g$
T_b	bed temperature
T_w	wall temperature
u_g	superficial gas velocity
x	size parameter; $x = 2\pi a/\lambda$
X	half-width of the cross-section in x- or y-direction

Greek symbols

β	extinction coefficient
δ_{sec}	voidage averaged over the cross-section
δ_a	voidage in the annular zone
ξ_a	thickness of the annular zone
η	the distance from the CFB centerline
θ	the angle between the incident and the outgoing beams
κ	absorption coefficient
λ	wavelength of incident radiation
ρ_g	gas density
σ	scattering coefficient
Φ	η/X

ash is released from the char matrix as the carbonaceous matter is gasified. Therefore, the particle properties (including the size and the material) change. The various types of particles entrained in the combustion gas can be classified as carbonaceous (coal, char and soot) or non-carbonaceous/inorganic (fly ash) [12]. The homogeneous spherical particles of coal and the coal combustion products have scattering properties which are significantly different.

In addition, silica sand is usually employed as bed material (heat transfer medium) and limestone is used to capture sulfur in CFB combustors. The complex refraction indexes differ significantly for various particles existing in CFB combustors. More attention must be paid to the properties of radiative media in CFB combustors since it is one of the essential parameters governing the scattering and absorption efficiency factors of the participating media [11].

The influence of the particle size on the radiation properties in CFB was studied before. Luan et al. [4] found nothing but a small effect of the mean particle size, probably because their study was limited to a narrow range (0.286–0.334 mm). On the contrary, others found (experimentally and numerically) [14–16] that the particle diameter is one of the most significant parameters and that the radiation heat transfer coefficient increases with the particle diameter.

This paper presents a 3D model predicting the bed-to-wall radiative heat transfer coefficient in the upper dilute zone of CFB combustors with rectangular cross-section. It is focused on the estimation of the influence of the particle properties (particle diameter, particle optical constants and solid composition) on the radiative heat transfer.

2. Optical constants of particle existing in CFB combustors

Coal, char, ash, sand and limestone particles exist simultaneously in the upper dilute zone of CFB combustors. The optical constants of these particles are reported in literature [12,13,17–22]. Since 80% fraction of radiation power is in the wavelength range 0.5–7 μm at about 850 °C, most attention must be paid to the optical constants for $\lambda < 7\,\mu m$.

(1) *Coal optical constants*

Brewster and Kunitomo [17] reviewed the results of research and concluded that the refractive index n and the absorption index k of coal are nearly constant in the wavelength range 0–20 μm. They gave the complex refractive index of coal [18]:

$$m = n - ik = 2.05 - 0.54i$$

(2) *Char optical constants*

Articles dealing with the measurement of char optical constants are rather scarce. So the values applied for complex refractive index of char were chosen from [18]:

$$m = n - ik = 2.20 - 1.12i$$

The influence of the complex refractive index on radiation will be discussed later.

(3) *Sand optical constants*

Sand, as the bed material, usually exists in the bottom bed of the CFB combustor. But since the combustor is operated at high gas velocity, the combustion gas may entrain some sand particles into the upper bed. Therefore, it is necessary to investigate the radiative heat transfer by sand. Lacroix et al. [19] measured the n and k values using the Kramers–Kronig transform of the signals. Their results are shown in Fig. 1. In the range 0–7 μm n varies from 1.5 to 1.1. The values of k also refer from [12] since it is hard to read the values by this figure.

(4) *Ash optical constants*

Im and Ahluwalia [12] analyzed the ash composition of Australian, Russian and US coals and found more than 50% of ash are made of silica. So the ash optical constants used in this paper are those given by Boothroyd and Jones [13], they are displayed in Table 1.

(5) *Limestone optical constants*

The optical constants of limestone were reported in two studies [17,20]. Querry et al.'s data (see Fig. 2) are used in this paper. There is an absorption peak at $\lambda = 7\,\mu m$.

Table 1
Optical constants of ash

λ	n	λ	$\log_{10}k$
0.5–6.0	1.5	0.5–1.0	$-4.6 + 2.2(\lambda - 0.5)$
6.0–8.0	$1.5 - 0.35(\lambda - 6.0)$	1.0–4.0	−3.5
8.0–11.0	$0.8 + 0.5(\lambda - 8.0)$	4.0–5.0	$-3.5 + (\lambda - 4.0)$
11.0–12.0	$2.3 - 0.5(\lambda - 11.0)$	5.0–7.5	$-2.5 + 0.24(\lambda - 5.0)$
		7.5–8.5	$-1.9 + 1.8(\lambda - 7.5)$
		8.5–10.5	−0.1
		10.5–12	$-0.1 - 0.733(\lambda - 10.5)$

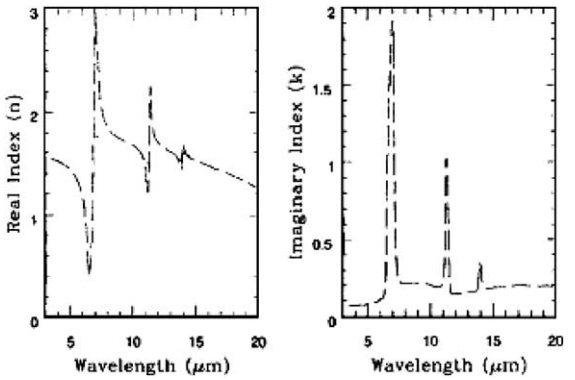

Fig. 2. Limestone optical constants, after [20].

3. Theory

3.1. Assumptions

The model is based on the following assumptions:

(1) The system is at steady state.
(2) There exists a core-annulus structure in the upper dilute zone.
(3) The particles are spherical.
(4) The fluidizing gas is a non-participating medium.
(5) The heat transfer surfaces and the bed wall are gray and diffuse surfaces.

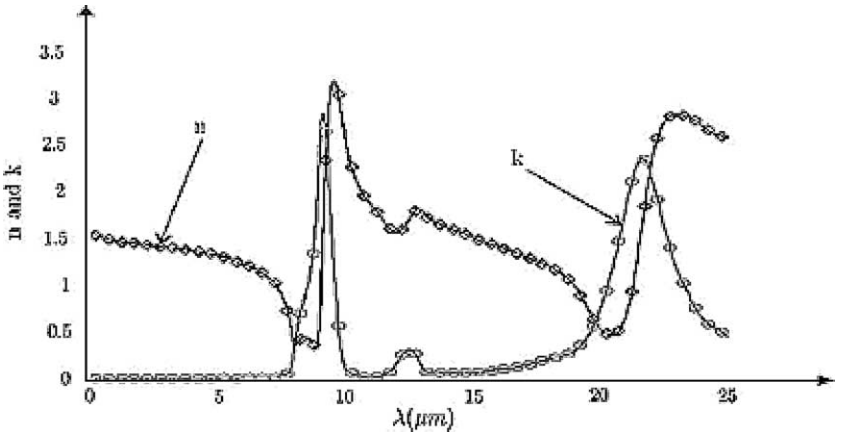

Fig. 1. Sand optical constants, after [19].

(6) The particle surfaces are large with respect to the radiation wavelength, and they are gray and diffuse surfaces. Scattering is independent and anisotropic, and the radiative properties of the particles do not change with temperature.
(7) The distribution of the solid volume fraction in the core zone is uniform on a horizontal cross-section, whereas it is non-uniform in the annular zone.

3.2. Hydrodynamic model and temperature distribution

The hydrodynamic model has been described before [23]. It is assumed that the cross-section of the core zone is rectangular. The thickness of the annular zone, ξ_a, at height h, is estimated as [24]:

$$\frac{\xi_a}{X} = 1 - \sqrt{1.34 - 1.30(1-\delta_{sec})^{0.2} + (1-\delta_{sec})^{1.4}} \tag{1}$$

where the gas film between the suspension phase and the bed wall is neglected; X is the half-width of the cross-section in x- or y-direction; and δ_{sec} is voidage averaged over the cross-section, estimated elsewhere [23].

The voidage distribution in the annular zone is determined as [25]:

$$\delta_a(\Phi) = \delta_{sec}^{0.191+\Phi^{2.5}+\Phi^{11}} \tag{2}$$

where $\Phi = \eta/X$ and η is the distance from the CFB centerline.

The temperature distribution is estimated on the basis of Golriz's correlation [26]:

$$\begin{aligned}\theta &= \frac{T - T_w}{T_b - T_w} \\ &= 1 - [-0.023Re_p + 0.163(T_b/T_w) + 0.294(h/H)] \\ &\quad \times \exp[-0.0054(x/d_p)]\end{aligned} \tag{3}$$

where T_b and T_w are the bulk suspension temperature and the wall temperature, respectively; h is the height above the distributor; H is the total height of the CFB riser; and Re_p is the particle Reynolds number defined as $u_g\rho_g d_p/\mu_g$.

3.3. Scattering and absorption coefficients

Mie theory is used to calculate the absorption and scattering efficiency factors of particles existing in CFB combustors. Boothroyd et al. [27] verified that this approach may be used in fluidized beds, and Gurvich et al. [28] verified its accuracy for large values of the size parameter ($x = 2\pi a/\lambda$). The initial version of the Mie code applied here is from [29]. For the application to particles in CFBs, we improved the code to the case of particles with wide size distribution. Satisfying tests were obtained for the following ranges of parameters (See also Appendix A)

Real refractive index n: 1.2–2.
Absorption index k: 10^{-5}–2.
Particle radius a: 1–2000 μm.

Based on the fourth and sixth assumptions above, the scattering and extinctive coefficients of the medium are given by [11]:

$$\begin{aligned}\sigma_\lambda &= N_T C_{sca} = \pi a^2 N_T Q_{sca} \\ &= \pi a^2 f_v \Big/ \left(\frac{4}{3}\pi a^3\right) Q_{sca} = \frac{3 f_v Q_{sca}}{4a} = \frac{3 f_v Q_{sca}}{2 d_p}\end{aligned} \tag{4}$$

$$\begin{aligned}\beta_\lambda &= N_T C_{ext} \\ &= \pi a^2 f_v \Big/ \left(\frac{4}{3}\pi a^3\right) Q_{ext} = \frac{3 f_v Q_{ext}}{4a} = \frac{3 f_v Q_{ext}}{2 d_p}\end{aligned} \tag{5}$$

$$g = \overline{\cos\theta} = \int_{-1}^{+1} \mu \cdot p(\mu)\, d\mu \tag{6}$$

where Q_{sca} and Q_{ext} are the scattering efficiency factor and the extinctive efficiency factor, respectively; f_v is the solid volume fraction; x is the size parameter and $x = 2\pi a/\lambda$; $\mu = \cos\theta$, θ is the angle between the incident and the outgoing beams and g the asymmetry factor.

Since scattering can be simplified as being independent in the upper zone of the CFB combustor [30], the coefficients of the clouds of particles of varying size and composition can be determined by summing over all single particles [31]:
Scattering coefficient:

$$\sigma = \sum_i C_{sca,i} N_i = \sum_i \frac{3 f_{v,i} Q_{sca,i}}{2 d_{p,i}} \tag{7}$$

Extinction coefficient:

$$\beta = \sigma + \kappa = \sum_i C_{ext,i} N_i = \sum_i \frac{3 f_{v,i} Q_{ext,i}}{2 d_{p,i}} \tag{8}$$

Asymmetry factor:

$$g = \sum_i f_{v,i} g_i \tag{9}$$

3.4. Numerical solution

The radiative transfer equation (RTE) is solved using the discrete ordinates method (DOM) [11,32]. In the method, the RTE along the propagation path, r, in the particle direction μ_i ($\mu_i = \cos\theta_i$), can be written as:

$$\begin{aligned}\mu_i \cdot \frac{dI}{dr}(r,\mu_i) &= -\beta \cdot I(r,\mu_i) + \kappa \cdot I_b(T_b) \\ &\quad + \frac{\sigma_s}{2} \sum_{j=1}^{n} I(r,\mu_j) \cdot p(\mu_j,\mu_i) \cdot \omega_j, \\ i &= 1,2,\ldots,n\end{aligned} \tag{10}$$

where $I_b(T_b)$ is the black body emission at T_b, $p(\mu_j, \mu_i)$ is the phase function and ω_j is the weight factor in μ_j direction and $p(\theta) = 8(\sin\theta - \theta\cos\theta)/3\pi$ is the phase function for large particles in fluidized beds [33]. All the results that are described hereafter were obtained using the LSO S6 quadrature set and the step scheme. The accuracy of the method was detailed in [34,35].

The radiative flux at any distance x from the wall in the bed can be obtained by integrating the local spectral radiation intensity, i.e.

$$q_r(x) = \int_0^\infty \left[2\pi \int_{-1}^{1} I_\lambda(x,\mu)\mu \, d\mu\right] d\lambda \tag{11}$$

where the wavelength ranges from 0 to ∞. In our work, since the bulk suspension temperature is lower than 850 °C, more than 99.5% of the thermal radiation from a blackbody lies within the wavelength range 0.5–21 μm.

Once $q_r(x)$ is calculated, the corresponding heat transfer coefficient is:

$$h_r = \frac{q_r(x=0)}{T_b - T_w} \tag{12}$$

In this study, a non-uniform grid was used: the grid is dense in the annular zone, especially near the bed walls since the voidage changes strongly at their vicinity. In the core zone, the grid is relatively sparse. All the results were obtained using a $70 \times 70 \times 30$ grid.

4. Validation of the model

4.1. Experimental data of Basu and Konuche [36]

Basu and Konuche [36] investigated the significance of the bed-to-wall radiation heat transfer in a 0.2 m × 0.2 m square and 6.7 m high CFB combustor. The probe was placed flush with the wall and 3.85 m above the air distributor. The superficial velocity was between 8 and 11 m/s at operating temperature. The bed material was sand of mean size 296 μm. The bed density was 20 kg/m^3. The emissivity of the exposed surface of the probe was about 0.97.

The sand optical constants employed in the model are from [19]. Fig. 3 shows the comparison of the model's prediction with experimental data. The error between the prediction and experiments is estimated as ±8%. It indicates that the theoretical results are in good agreement with experimental data in the temperature range, 650–900 °C.

4.2. Experimental data of Han and Cho [37]

Han and Cho [37] experimented a 6.0 m high facility with 0.2 m × 0.2 m rectangular cross-section. The bed temperature was in the range 650–850 °C, the superficial gas velocity was 3.0–5.0 m/s and the measured suspension density was 20–30 kg/m^3. The suspension emissivity determined from the radiation probe was in range 0.7–0.98. The radiation probe was placed flush with the wall and 3.5 m above the distribution plate. The mean particle size of coal was 1.3 mm.

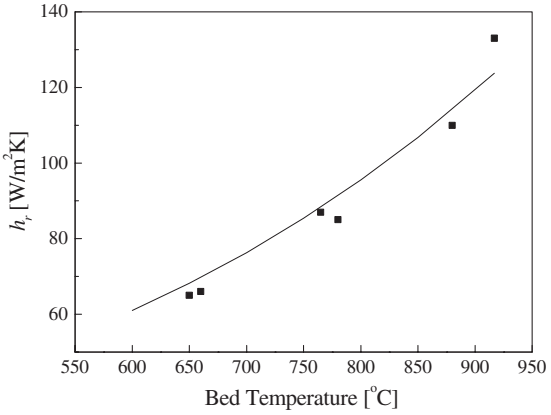

Fig. 3. Comparison of the predicted results with experimental data [36]: (■) experimental data; (—) results predicted by the model.

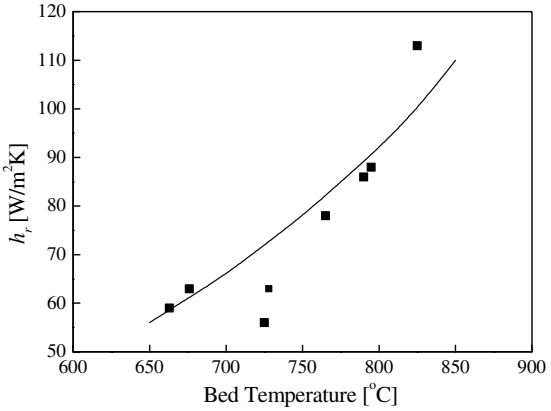

Fig. 4. Comparison of the predicted results with experimental data [37]: (■) experimental data; (—) results predicted by the model.

The optical constant of anthracite is 2.05–0.54i [18] (the ash fraction is neglected since the probe position is low). The expected error between the prediction and experiments is ±18%. The results predicted by the model are compared with experimental data in Fig. 4, and the comparison is satisfactory in the temperature range.

5. Results and discussion

The theoretical investigation is carried out on a 1.7 m × 1.4 m cross-section and 13.5 m high CFB

combustor. The superficial velocity is 3.2 m/s. The bed temperature is 850 °C and the wall temperature is 400 °C. The influence of the particle properties on the radiative heat transfer coefficient is studied.

Firstly, the influence of the coal particle diameter on the radiative heat transfer coefficient is studied since it changes along the height of the CFB combustor. Considering three groups of uniform coal particles with different mean diameters (0.2 mm; 0.3 mm; 0.4 mm), the radiative heat transfer coefficient changes significantly with the particle diameter (Fig. 5). This was also reported by others [14–16]. Smaller particles (at the same voidage) act as a denser shield between the high bed temperature and the wall, thus decreasing the net radiation flux.

Secondly, the influence of the particle size distribution is studied since the particle size is widely distributed in CFB combustors [23]. Fig. 6 shows the existing particle size distribution in a CFB combustor, as used here. Fig. 7 plots the predicted results for solid with Gaussian-type of particle size distribution and Sauter mean diameter. It shows that the Sauter mean diameter can be substituted to the particle size distribution in calculations. We also studied the cases of solid with flat particle size distribution and binary mixture and similar results were obtained. Comparing the expression of Sauter mean diameter ($\bar{d} = (\sum \frac{f_i}{d_i})^{-1}$) with Eqs. (4) and (5), we can see that if there is not great difference between the absorption and scattering efficiency factors, thus the Sauter mean diameter can be used in calcula-

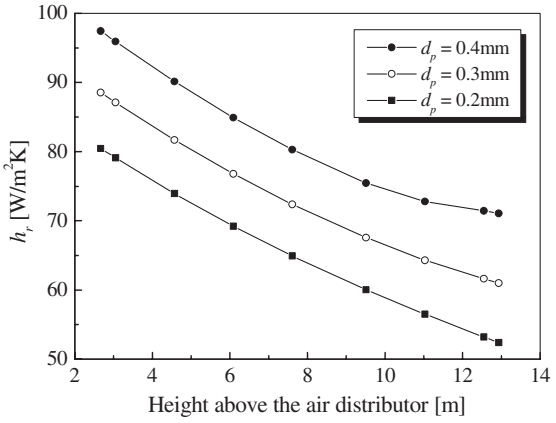

Fig. 5. Influence of the particle diameter on the radiative heat transfer coefficient: T_b = 850 °C; T_w = 400 °C; type of particle: coal (m = 2.05 − 0.54i).

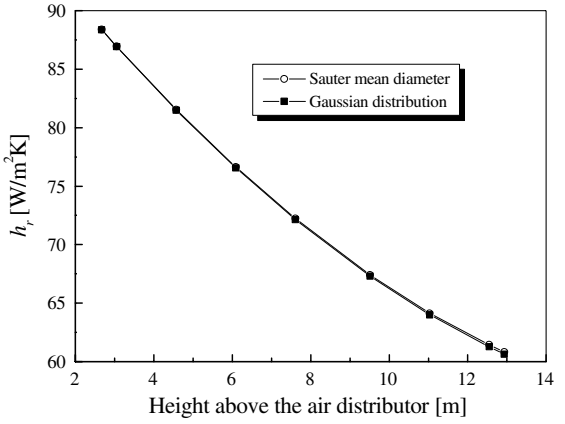

Fig. 7. Influence of Gaussian-type particle size distribution on the radiative heat transfer: T_b = 850 °C; T_w = 400 °C; type of particle: coal (m = 2.05 − 0.54i).

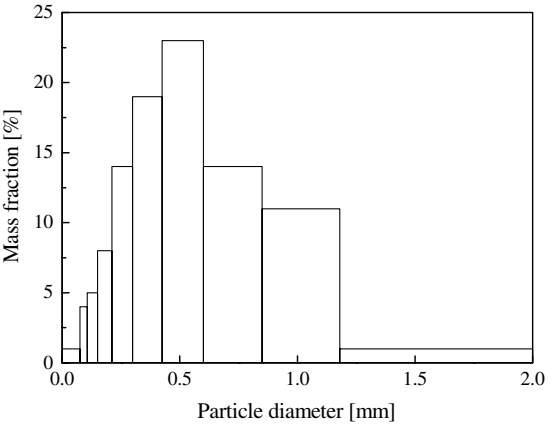

Fig. 6. Particle size distribution in CFB combustor.

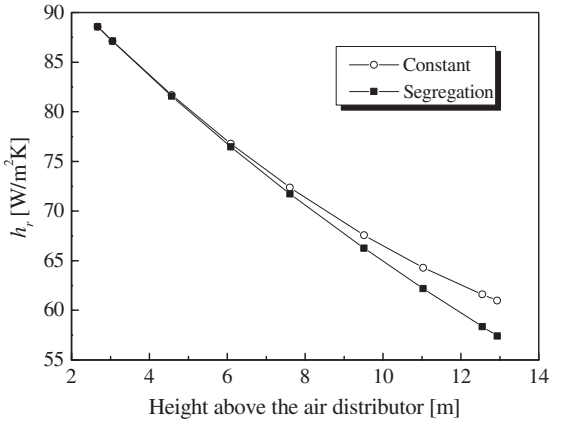

Fig. 8. Influence of the axial solid segregation on the radiative heat transfer: T_b = 850 °C; T_w = 400 °C; type of particle: coal (m = 2.05 − 0.54i).

tions for particles with wide size distribution. But it can be applied only for particles with similar optical constants and distribution in the range 100–1000 μm (see Appendix A). For other systems (e.g. pulverized coal-fired systems), this rule may not be appropriate [38].

Thirdly, the influence of the axial solid segregation on the radiative heat transfer is investigated here since it always exists in CFB combustors [23]. The mean particle diameter is supposed to decrease from 0.3 mm to 0.18 mm along the height in this case, whereas the particle size is assumed to be uniform horizontally. The radiative heat transfer decreases in the upper part of the bed when solid segregation occurs (Fig. 8).

The results concerning the influence of optical constants on the radiative heat transfer are presented hereafter. Marakis et al. [39] investigated the influence of the real part of the optical constant, i.e. the refractive index (n) and of the imaginary part, i.e. the absorption index (k) of ash. They found that the absorption coefficient has more influence on the heat transfer coefficient than the refractive index. But their results are unilateral because of the narrow range of the indexes. In our study, wide ranges of absorption index (k) and of refractive index (n) are considered. Results plotted in Fig. 9 show that the radiative heat transfer coefficient increases strongly with k when in the range $10^{-3} < k < 5 \times 10^{-3}$ (about 50%), then it plateaus whilst k varies of 2 orders of magnitude, until it starts decreasing as soon as k becomes larger than 1. For a given absorption index, the radiative heat transfer coefficient increases slightly with the refractive index, and the influence is less sensitive near $k = 1$. Fig. 10 indicates that the influence of n is weak when k is great, with a maximal value of the heat transfer coefficient for $n \approx 1.5$. When k is small, the radiative heat transfer coefficient increases significantly (≈10–15%) when n increases from 0.5 to 1, then it decreases slightly. Clearly, the two indexes influence each other.

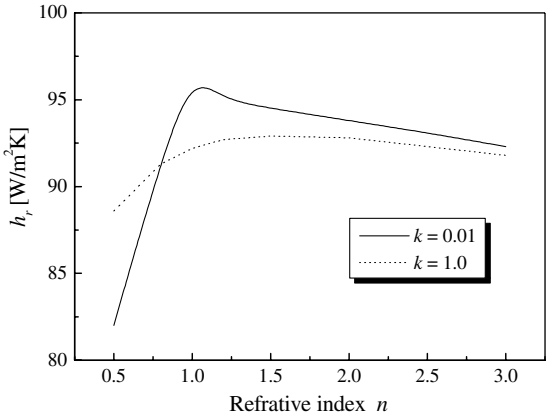

Fig. 10. Influence of the refractive index on the radiative heat transfer coefficient: $T_b = 850\,°C$; $T_w = 400\,°C$; probe position: $h = 4.5\,m$ ($f_v = 1.3\%$).

Table 2
Particle composition in CFB combustor for simulation (reference Case 1)

Particle kind	Fraction (splash zone)	Fraction (top)	Mean diameter (mm)
Sand	10%	0	0.5
Coal	10%	0	0.5
Char	60%	10%	0.3
Ash	10%	80%	0.1
Limestone	10%	10%	0.2

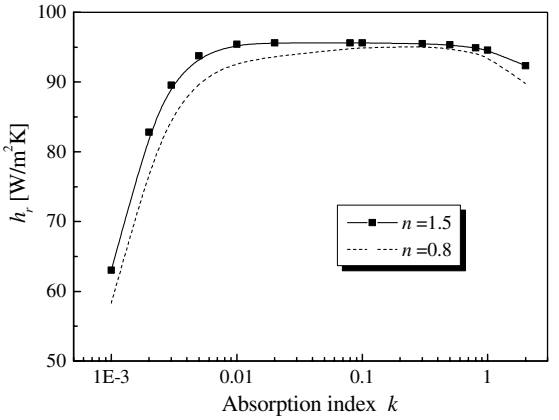

Fig. 9. Influence of the absorption index on the radiative heat transfer coefficient: $T_b = 850\,°C$; $T_w = 400\,°C$; probe position: $h = 4.5\,m$ ($f_v = 1.3\%$).

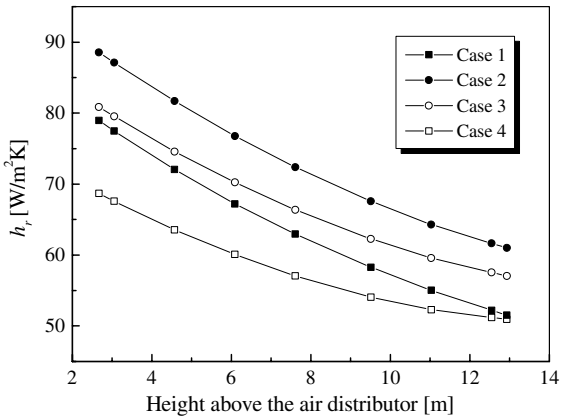

Fig. 11. Influence of the solid composition on the radiative heat transfer coefficient: $T_b = 850\,°C$; $T_w = 400\,°C$; Case 1: particle mixture in Table 2; Case 2: char; Case 3: ash; Case 4: sand.

Table 3
Sensitivity analysis of parameters on the radiative heat transfer coefficient

	Hydrodynamic parameters				Temperature field			
	δ_{sec}		ξ_a		$T_b = 850\,°C$		$T_w = 400\,°C$	
Parameter variation	+10%	−10%	+10%	−10%	+50 °C	−50 °C	+50 °C	−50 °C
h_r variation	−1%	+2%	−0.05%	+0.1%	+3%	−4%	+15%	−15%

Finally, the case of a bed composed of sand, coal, char, ash and limestone in the upper zone is studied. Since most of the sand remains in the bottom bed, its fraction is supposed to decrease from 10% to 0 from the splash zone to the top. Its mean diameter is assumed to be 0.5 mm. Most coal particles change into char in the bottom bed, so the coal's fraction is supposed to decrease from 10% to 0 from the splash zone to the top. Its mean diameter is 0.5 mm. The fraction of char decreases from 60% (splash zone) to 10% (top). Its mean diameter is 0.3 mm. The fraction of ash increases from 10% (splash zone) to 70% (top). Its mean diameter is 0.10 mm. According to the operation conditions the Ca/S molar ratio is 2. Therefore, we suppose the fraction of limestone remains at 10% along the height and its diameter is 0.2 mm. Table 2 summarizes this set of values. This composition (Case 1) is compared with three other cases, corresponding to extreme conditions:

Case 2: All particles are char.
Case 3: All particles are ash.
Case 4: All particles are sand.

The results are plotted in Fig. 11. The radiative heat transfer coefficient is always higher when all particles are char (Case 2); on the contrary, it is always lower when all particles are sand (Case 4) because of the influence of the absorption index k. Up to 25% error may be done on the calculation of the radiative heat transfer coefficient depending on the solid composition, just because of the variation of the optical properties of the particles.

6. Sensitivity analysis

A sensitivity analysis was performed to investigate the influence of the voidage averaged over the cross-section, δ_{sec}, the thickness of the annular zone, ξ_a and of the temperature field on the radiative heat transfer coefficient (h_r). The results of this sensitivity analysis are displayed in Table 3. It shows that the hydrodynamic parameters have a very weak influence on the radiative heat transfer coefficient, whereas the bed and wall temperature do have a strong influence on it. These results point out that both the wall and bed temperatures must be known very accurately for good estimation of the radiative heat transfer coefficient. On the contrary, big uncertainties on the voidage and on the annular thickness are permitted, since they have little effect on the estimation of the radiative heat transfer coefficient.

7. Conclusions

The particle diameter has a significant influence on the bed-to-wall radiative heat transfer coefficient. Smaller particles (at the same voidage) act as a denser shield between the high bed temperature and the wall, thus decreasing the net radiation flux. The Sauter mean diameter can be applied to calculate the radiative heat transfer coefficient for polydispersions with wide size distribution. But two conditions are necessary: (1) the polydispersions must have similar optical constants; (2) most particles must be greater than 100 μm. The solid segregation has some influence on the radiative heat transfer coefficient.

The solid composition plays an important role on the radiative heat transfer coefficient because of the influence of real and imaginary parts of complex refractive index on particulate optical properties. In order to calculate the radiative heat transfer coefficient more accurately, more research must be done on the optical constants of particles existing in CFBs, and the knowledge of the solid composition in different positions in the combustor must be improved.

Acknowledgments

This work was developed within the frame of the Sino-French Collaboratory of Chemical and Environmental Engineering for Sustainable Development. Authors are grateful to the French Embassy in Beijing (Service de Coopération et d'Action Culturelle) for financially supporting the Sino-French co-advised thesis of one of the authors (Y. Hua).

Appendix A. Application of Mie theory for the CFB combustor particles ($\lambda = 4.0\,\mu m$)

Q_{ext} values

			$k = 10^{-5}$	$k = 10^{-4}$	$k = 10^{-3}$	$k = 10^{-2}$	$k = 0.1$	$k = 1.0$	$k = 2.0$
$n = 1.2$	$a = 1$	$x = 1.571$	0.1309	0.1313	0.1353	0.1753	0.5464	2.5770	3.4754
	$a = 10$	$x = 15.71$	2.2484	2.2490	2.2554	2.3044	2.2872	2.3124	2.4651
	$a = 100$	$x = 157.1$	2.0538	2.0553	2.0553	2.0684	2.0614	2.0704	2.0883
	$a = 1000$	$x = 1571$	2.0141	2.0142	2.0147	2.0147	2.0140	2.0150	2.0167
	$a = 2000$	$x = 3142$	2.0075	2.0076	2.0081	2.0080	2.0077	2.0082	2.0090
$n = 2.0$	$a = 1$	$x = 1.571$	4.2203	4.2196	4.2132	4.1512	3.6914	2.9561	3.1508
	$a = 10$	$x = 15.71$	2.4175	2.4156	2.3971	2.3123	2.2998	2.3242	2.3929
	$a = 100$	$x = 157.1$	2.0708	2.0709	2.0704	2.0671	2.0674	2.0736	2.0865
	$a = 1000$	$x = 1571$	2.0095	2.0122	2.0147	2.0147	2.0147	2.0155	2.0168
	$a = 2000$	$x = 3142$	2.0091	2.0080	2.0081	2.0081	2.0081	2.0084	2.0091

Q_{sca} values

			$k = 10^{-5}$	$k = 10^{-4}$	$k = 10^{-3}$	$k = 10^{-2}$	$k = 0.1$	$k = 1.0$	$k = 2.0$
$n = 1.2$	$a = 1$	$x = 1.571$	0.1308	0.1308	0.1306	0.1286	0.1358	0.9458	1.9055
	$a = 10$	$x = 15.71$	2.2478	2.2432	2.1983	1.8463	1.1338	1.3598	1.7140
	$a = 100$	$x = 157.1$	2.0486	2.0042	2.0042	1.0788	1.0738	1.2933	1.5437
	$a = 1000$	$x = 1571$	1.9637	1.6195	1.0605	1.0536	1.0593	1.2624	1.5005
	$a = 2000$	$x = 3142$	1.9106	1.3844	1.0508	1.0507	1.0565	1.2584	1.4958
$n = 2.0$	$a = 1$	$x = 1.571$	4.2201	4.2185	4.2022	4.0454	2.9469	1.3216	1.6670
	$a = 10$	$x = 15.71$	2.4163	2.4041	2.2960	1.7672	1.2472	1.3513	1.5752
	$a = 100$	$x = 157.1$	2.0649	2.0136	1.6506	1.1971	1.1959	1.2841	1.4552
	$a = 1000$	$x = 1571$	1.9504	1.5952	1.1728	1.1710	1.1720	1.2562	1.4194
	$a = 2000$	$x = 3142$	1.8965	1.3927	1.1676	1.1676	1.1686	1.2525	1.4153

References

[1] P. Basu, Heat transfer in high temperature fast fluidized beds, Chem. Eng. Sci. 45 (1990) 3123–3136.

[2] G. Flamant, J.D. Lu, B. Variot, Towards a generalized model for vertical walls to gas–solid fluidized bed heat transfer—II. Radiative transfer and temperature effects, Chem. Eng. Sci. 48 (1993) 2493–2503.

[3] K. Kudo, H. Taniguchi, H. Kaneda, W. Yang, Y. Zhang, K.H. Guand, M. Matsumura, Flow and heat transfer simulation in circulating fluidized beds, in: P. Basu, M. Horio, M. Hasatani (Eds.), Circulating Fluidized Bed Technology III, Pergamon Press, Oxford, 1991, pp. 269–274.

[4] W. Luan, C.J. Lim, C.M.H. Brereton, B.D. Bowen, J.R. Grace, Experimental and theoretical study of total and radiative heat transfer in circulating fluidized beds, Chem. Eng. Sci. 54 (1999) 3749–3764.

[5] P. Basu, P.K. Nag, An investigation into heat transfer in circulating fluidized beds, Int. J. Heat Mass Transfer 30 (1987) 2399–2409.

[6] C. Werdermann, J. Werther, Heat transfer in large-scale circulating fluidized bed combustors of different sizes, in: A.A. Avidan (Ed.), Circulating Fluidized Bed Technology IV, AIChE, New York, 1994, pp. 428–435.

[7] A. Glatzer, W. Linzer, Radiative heat transfer in circulating fluidized beds, in: J.F. Large, C. Laguérie (Eds.), Fluidization VIII, Engineering Foundation, New York, 1995, pp. 311–318.

[8] Z.H. Fang, J.R. Grace, C.J. Lim, Radiative heat transfer in circulating fluidized beds, J. Heat Transfer 117 (1995) 963–968.

[9] A.P. Baskakov, B. Leckner, Radiative heat transfer in circulating fluidized bed furnaces, Powder Technol. 90 (1997) 213–218.

[10] D. Xie, B.D. Bowen, J.R. Grace, C.J. Lim, Two-dimensional model of heat transfer in circulating fluidized beds. Part I: Model development and validation, Int. J. Heat Mass Transfer 46 (2003) 2179–2191.

[11] M.F. Modest, Radiative Heat Transfer, McGray-Hill, New York, 1993.

[12] K.H. Im, R.K. Ahluwalia, Radiation properties of coal combustion products, Int. J. Heat Mass Transfer 36 (1993) 293–302.

[13] S.A. Boothroyd, A.R. Jones, A comparison of radiative characteristics for fly ash and coal, Int. J. Heat Mass Transfer 29 (1986) 1649–1654.

[14] J. Yamada, Y. Kurosaki, T. Morikawa, Radiation emitted from fluidizing particles adjacent to a heated surface in a fluidized bed, Int. J. Therm. Sci. 40 (2001) 104–113.

[15] Q. He, F. Winter, J. Lu, Analysis of the heat transfer mechanism in high-temperature circulating fluidized beds by numerical model, J. Energy Resour. Technol. 124 (2002) 34–39.
[16] D. Xie, B.D. Bowen, J.R. Grace, C.J. Lim, Two-dimensional model of heat transfer in circulating fluidized beds. Part I: Heat transfer in a high density CFB and sensitivity analysis, Int. J. Heat Mass Transfer 46 (2003) 2193–2205.
[17] M.Q. Brewster, T. Kunitomo, The optical constants of coal, char, and limestone, J. Heat Transfer 106 (1984) 678–683.
[18] R. Vistanta, A. Ungan, M.P. Menguç, Predictions of radiative properties of pulverized coal and fly-ash polydispersions, ASME paper no. 81-HT-24, 1981.
[19] D. Lacroix, G. Parent, F. Asllanaj, G. Jeandel, Coupled radiative and conductive heat transfer in a non-grey absorbing and emitting semitransparent media under collimated radiation, J. Quant. Spectros. Radiat. Transfer 75 (2002) 589–609.
[20] M.R. Querry, G. Osborne, K. Lies, R. Jordon, R.M.Jr. Coveney, Complex refractive index of limestone in the visible and infrared, Appl. Optics 17 (1978) 353–356.
[21] M.P. Menguç, B.W. Webb, Radiative heat transfer, in: Fundamental of Coal Combustion, Elsevier, Amsterdam, 1993.
[22] A.G. Blokh, Heat Transfer in Steam Boiler Furnaces, Hemisphere, Washington, DC, 1988.
[23] Y. Hua, G. Flamant, J. Lu, D. Gauthier, Modelling of axial and radial solid segregation in a CFB boiler, Chem. Eng. Process 43 (2004) 971–978.
[24] X.T. Bi, J. Zhou, S.Z. Qin, J.R. Grace, Annular wall layer thickness in circulating fluidized bed risers, Can. J. Chem. Eng. 74 (1996) 811–814.
[25] W. Zhang, Y. Tung, F. Johnsson, Radial voidage profiles in fast fluidized beds of different diameters, Chem. Eng. Sci. 46 (1991) 3045–3052.
[26] M.R. Golriz, An experimental correlation for temperature distribution at the membrane wall of CFB boilers, in: K.J. Heinschel (Ed.), Proc. 13th Int. Fluidized Bed Combustion Conf., vol. 1, 1995, pp. 499–505.
[27] S.A. Boothroyd, A.R. Jones, K. Nicholson, W.R. Wood, Light scattering by fly ash and the applicability of Mie theory, Comb. Flame 69 (1987) 235–241.
[28] I. Gurvich, N. Shiloah, M. Kleiman, Calculations of the Mie scattering coefficients for multilayered particles with large size parameters, J. Quant. Spectros. Radiat. Transfer 70 (2001) 433–440.
[29] C.F. Bohren, D.R. Huffman, Absorption and Scattering of Light by Small Particles, John Wiley & Sons, New York, 1998, pp. 477–482.
[30] C.L. Tien, B.L. Drolen, Thermal radiation in particulate media with dependent and independent scattering, in: Annual Review of Numerical Fluid Mechanics and Heat Transfer, vol. 1, Hemisphere, New York, 1987, pp. 1–32.
[31] M.Q. Brewster, Thermal Radiative Transfer and Properties, Wiley, New York, 1992.
[32] W.A. Fiveland, Three-dimensional radiative heat-transfer solutions by the discrete-ordinates method, J. Thermophys. Heat Transfer 2 (1988) 309–316.
[33] C.L. Tien, Thermal radiation in packed and fluidized beds, J. Heat Transfer 110 (1988) 1230–1242.
[34] H. Li, G. Flamant, J. Lu, An alternative discrete ordinate scheme for collimated irradiation problems, Int. Comm. Heat Mass Transfer 30 (2003) 61–70.
[35] H. Li, G. Flamant, J. Lu, Investigation of the ray effects in the discrete ordinate method, Numer. Heat Transfer, Part B 43 (2003) 445–466.
[36] P. Basu, F. Konuche, Radiative heat transfer from a fast fluidized bed, in: P. Basu, J.F. Large (Eds.), Circulating Fluidized Bed Technology II, Pergamon press, 1988, pp. 245–253.
[37] G.Y. Han, Y.J. Cho, Radiative heat transfer in a circulating fluidized bed coal combustor, Powder Technol. 102 (1999) 266–273.
[38] F. Liu, The effects of particle size distribution and refractive index on fly-ash radiative properties using a simplified approach, Int. J. Heat Mass Transfer 36 (1993) 1905–1912.
[39] J.G. Marakis, G. Brenner, F. Durst, Monte Carlo simulation of a nephelometric experiment, Int. J. Heat Mass Transfer 44 (2001) 989–998.